



OPEN RSL3 induces ferroptosis by activating the NF- κ B signalling pathway to enhance the chemosensitivity of triple-negative breast cancer cells to paclitaxel

Jialin Yuan¹, Cong Liu¹, Chengwei Jiang², Ning Liu¹✉, Zhaoying Yang¹✉ & Hua Xing¹✉

Chemotherapy resistance in triple-negative breast cancer (TNBC) leads to poor therapeutic effects and a poor prognosis. Given that paclitaxel-based chemotherapy is the main treatment method for TNBC, enhancing its chemosensitivity has been a research focus. Induced ferroptosis of tumour cells has been proven to increase chemosensitivity, but its ability to sensitize TNBC cells to paclitaxel (PTX) is unknown. In our experiments, measurements of viability and proliferation validated the synergistic effect of PTX combined with RSL3 on TNBC cells. The accumulation of intracellular Fe²⁺ and lipid reactive oxygen species, as well as the expression of malondialdehyde, illustrated that RSL3 enhanced the chemosensitivity of TNBC to PTX by inducing ferroptosis. Through transcriptome sequencing, a series of differentially expressed genes were identified, in which the expression of cytokines, such as CXCLs, was significantly increased in the treatment group, and the effect of combination therapy on TNBC was enriched mainly in the NF κ B signalling pathway. In subsequent validation experiments, the use of the NF- κ B inhibitor BAY11-7082 reversed the inhibitory effects of PTX and RSL3 on TNBC cell activity. In a xenograft immunodeficient mouse model, the inhibitory effects of PTX and RSL3 on TNBC *in vivo* were further verified. Our research validated the synergistic effects of PTX and RSL3 both *in vivo* and *in vitro*, with RSL3 inducing ferroptosis by activating the NF- κ B signalling pathway, thereby increasing the chemosensitivity of TNBC to PTX. This study provides new insights for improving the therapeutic efficacy of treatment strategies.

Keywords Triple-negative breast cancer, Ferroptosis, Chemosensitivity

Breast cancer poses a significant threat to women's health, with high incidence, mortality rate, and debilitating effects on patients' quality of life. According to the International Agency for Research on Cancer, a subordinate institution of the WHO, the number of newly diagnosed breast cancer cases globally reached 2.3 million in 2022, making it the second most common cancer worldwide. The National Cancer Centre of China recently reported that 357,200 cases of breast cancer occur annually, with 75,000 annual deaths. In addition, in China, breast cancer is characterized by a relatively young age of onset, a high malignancy rate, and poor prognosis.

Commonly recognized as a heterogeneous disease, diverse types of breast cancer are closely related to disease progression, treatment, and prognosis. Four major molecular subtypes of breast cancer have been identified via gene expression profiling analysis, i.e., Luminal A, Luminal B, HER2+, and triple-negative breast cancer (TNBC)¹. Adjuvant therapy for each subtype varies due to their pathological characteristics, with Luminal A patients requiring mainly endocrine therapy and Luminal B and HER2+ patients receiving conventional chemotherapy combined with endocrine and targeted therapy².

TNBC, a subtype of breast cancer with a high recurrence rate, high invasive metastasis rate, and poor prognosis, accounts for 15–20% of all breast cancer cases³. Since this subtype does not express the oestrogen receptor, progesterone receptor, or HER2 receptor, the main treatment is anthracycline and taxane chemotherapy⁴, but the pathological complete remission (pCR) rate of patients is only 30%–53%⁵. Moreover, there are a series of chemotherapy side effects in patients, such as nausea, vomiting, hair loss, myelosuppression,

¹Department of Breast Surgery, China-Japan Union Hospital of Jilin University, Changchun, China. ²Department of Pathology, China-Japan Union Hospital of Jilin University, Changchun, China. ✉email: ms008@jlu.edu.cn; zyyang@jlu.edu.cn; xingh@jlu.edu.cn

and the development of chemotherapy resistance, which are the main reasons for poor diagnostic outcomes and prognoses⁶. Considering the therapeutic status of paclitaxel (PTX) in TNBC and chemotherapy resistance, research on how to increase the chemosensitivity of TNBC to PTX has been extensively conducted in recent years. Therefore, the focus of this research is determining how to increase the chemosensitivity of TNBC to PTX.

Ferroptosis, a form of iron-dependent regulatory cell death (RCD) proposed by Professor Brent Stockwell in 2012, differs from apoptosis, necrosis, and autophagy in terms of morphology, biochemistry, and genetics⁷. In terms of cell morphology, ferroptosis leads to smaller mitochondria, increased membrane density, and decreased cristae. The composition of cells is characterized by elevated lipid reactive oxygen species (ROS), the core mechanism of which is the imbalance between oxidative damage and antioxidant defence^{7,8}. It has been reported that TNBC cells exhibit a unique metabolic balance of iron and glutathione, where the expression of genes involved in ferroptosis-related metabolic pathways (such as lipid, iron, and amino acid metabolism) is altered in TNBC, increasing the susceptibility of refractory tumours to ferroptosis⁹. Ferroptosis is another crucial form of cell death elicited by various cancer therapies, including chemotherapy, radiotherapy, immunotherapy, and targeted therapy^{10–13}. PTX can induce ferroptosis in lung, head and neck, colorectal, gastric, and pancreatic cancer cells¹⁴. Additionally, RSL3, an effective ferroptosis inducer, can directly inhibit glutathione peroxidase (GPX4) to induce ferroptosis in TNBC cells¹⁵. Consequently, ferroptosis inducers have great potential in cancer treatment, particularly when combined with conventional therapies^{10,16,17}. However, few studies have investigated the combined effects of RSL3 and PTX on TNBC. Therefore, our research aimed to explore whether the combination of PTX and RSL3 enhances the chemosensitivity of TNBC to PTX.

NF- κ B, a transcription factor that mediates a variety of biological processes, is involved in regulating cell proliferation and survival, the stress response, inflammation and the immune response¹⁸. The NF- κ B signalling pathway is a complex and crucial regulatory mechanism, and the classic NF- κ B signalling pathway has been widely proven to be essential in the regulation of the proliferation of malignant tumours¹⁹. Currently, the NF- κ B signalling pathway is known to be involved in ferroptosis, where the classic signalling pathway is activated by inflammatory factors, such as Toll-like receptor ligands (e.g., LPS), TNE, and IL-1²⁰. Moreover, NF- κ B can reduce the transcription of antioxidant molecules, such as GPX4, NQO1, and HMOX1, as well as participate in oxidative stress and induce ferroptosis²⁰. Therefore, interfering with ferroptosis, with the NF- κ B signalling pathway being a target, might be a potentially effective measure to enhance the chemosensitivity of TNBC to PTX.

In this study, we found that combination therapy of PTX and RSL3 promoted the death of MDA-MB-231 and MDA-MB-468 TNBC cells, resulting in decreased cell viability, reduced cell migration and invasion, and the accumulation of lipid peroxide products. Notably, our study demonstrates, for the first time, that RSL3 induces ferroptosis by activating the NF- κ B signalling pathway to enhance the chemosensitivity of TNBC to PTX.

Results

RSL3 enhances chemosensitivity of TNBC to PTX in vitro

PTX, a taxane chemotherapy drug, plays an important role in the treatment of TNBC. Interfering with the microtubule structure and function of tumour cells can prevent normal mitosis, thereby inhibiting the proliferation and spread of cancer cells. RSL3 is an effective ferroptosis inducer that can directly inhibit GPX4 and induce ferroptosis in TNBC cells. Therefore, in this study, TNBC cell lines (MDA-MB-231 and MDA-MB-468) were treated with various concentrations of PTX (0, 5, 50, 500 nM) combined with different concentrations of RSL3 (0, 0.1, 0.5, 1.5 μ M) for 24 h, and cell viability was assessed using a CCK-8 assay (Fig. 1A and B). Compared with PTX alone, the combination of PTX and RSL3 significantly inhibited the viability of MDA-MB-231 and MDA-MB-468 cells. The synergistic effect of the drug combination was evaluated via SynergyFinder software²¹, which revealed that the MDA-MB-231 HSA score was 18.7 and the MDA-MB-468 HSA score was 17.673 (Supplementary Fig. S1a and b). Both scores were greater than 10, demonstrating a synergistic sensitization effect of PTX and RSL3. The IC₅₀ values of RSL3 were calculated by fitting curves using Graphpadprism8 software, which revealed that the IC₅₀ of RSL3 in MDA-MB-231 cells was 2.668 μ M, whereas that in MDA-MB-468 cells was 0.5329 μ M. We selected a drug concentration of 20% of the IC₅₀ of RSL3 for subsequent sensitization experiments (Supplementary Fig. S2). The MDA-MB-231 cells were subsequently treated with PTX (5 nM), RSL3 (0.5 μ M) or their combination for 24 h, whereas the MDA-MB-468 cells were treated with PTX (5 nM), RSL3 (0.1 μ M) or their combination for 24 h. Next, to investigate whether RSL3 enhances the anti-proliferative effects of PTX on MDA-MB-231 and MDA-MB-468 cells, a colony formation assay was performed. Compared with PTX or RSL3 alone, the combination treatment significantly inhibited the proliferation of TNBC cells (Fig. 1C). In summary, RSL3 enhances the cytotoxic effects of PTX on TNBC cells by significantly inhibiting cell viability and cell proliferation.

The strong ability of cells to be invasive and metastasize contribute to a poor prognosis. Transwell migration and invasion assays were performed to determine the ability of RSL3 to enhance the inhibitory effect of PTX on the invasion and metastasis of TNBC cells. Compared with PTX or RSL3 alone, the combination of PTX and RSL3 significantly inhibited the migration of both MDA-MB-231 and MDA-MB-468 cells (Fig. 1D and E). Transwell invasion assays also revealed that the combination treatment enhanced the inhibition of tumour invasion (Fig. 1F and G). In summary, RSL3 enhanced the inhibitory effect of PTX on the migration and invasion of TNBC cells.

RSL3 enhances the chemosensitivity of TNBC cells to PTX by inducing ferroptosis

It has been reported that RSL3, an effective ferroptosis activator, can increase sensitivity to chemotherapy by inducing ferroptosis^{10,16,17}. To investigate whether the combination of PTX and RSL3 further promote ferroptosis, we combined several different types of cell death inhibitors with PTX and RSL3 in MDA-MB-231 and MDA-MB-468 cells and examined cell viability. These inhibitors include the apoptosis inhibitor Ac-

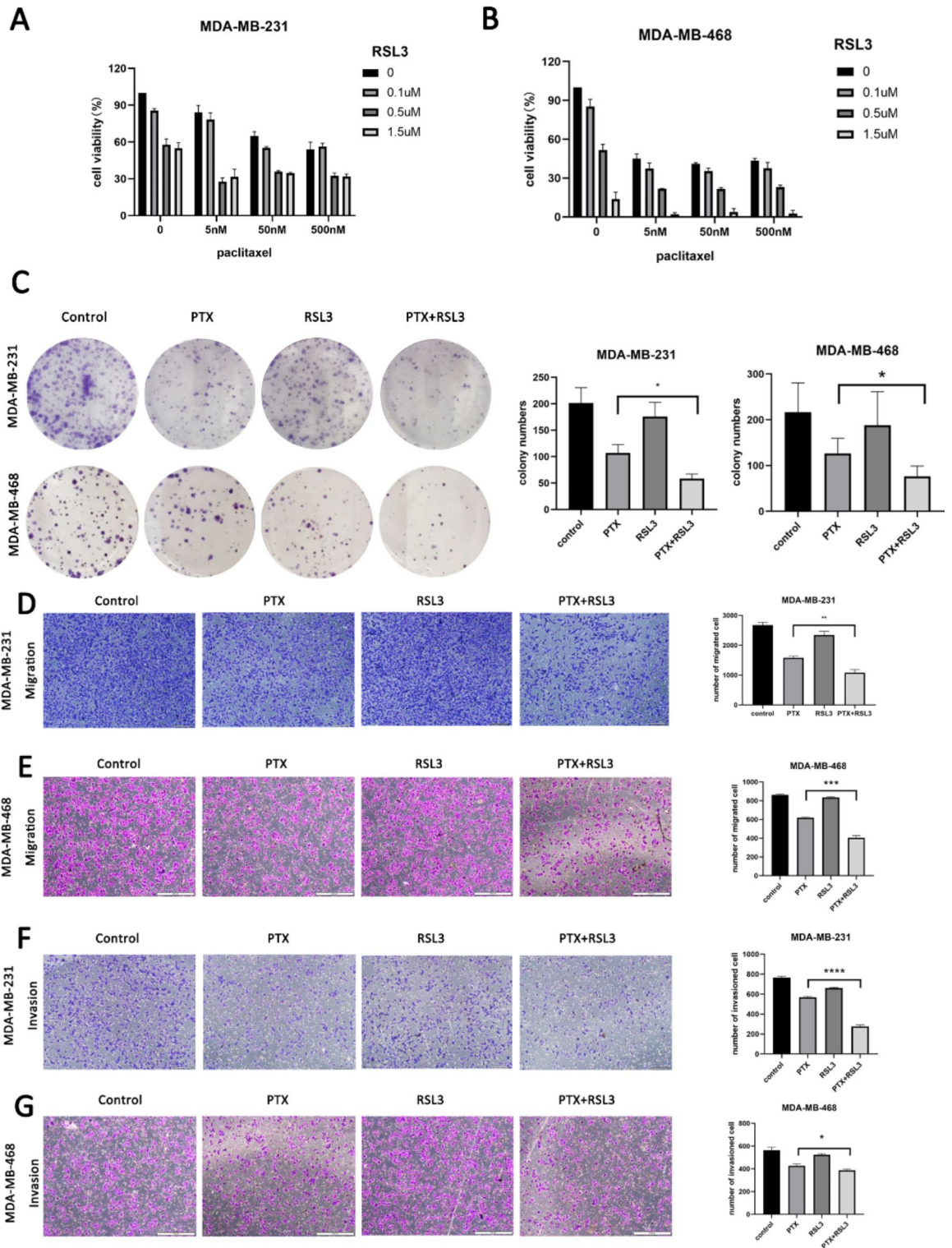


Fig. 1. RSL3 Enhances the Chemosensitivity of TNBC to PTX in vitro. (A, B) TNBC MDA-MB-231 and MDA-MB-468 cells were treated with various concentrations of PTX (0, 5, 50, 500 nM) combined with different concentrations of RSL3 (0, 0.1, 0.5, 1.5 μM) for 24 h, and cell viability was assayed using the CCK-8 assay. (C) Colony formation experiments were performed on MDA-MB-231 cells treated with PTX (5 nM), RSL3 (0.5 μM) or their combination for 24 h and on MDA-MB-468 cells treated with PTX (5 nM), RSL3 (0.1 μM) or their combination for 24 h. A histogram showing colony formation is presented. (D–G) Migration and invasion of treated cells were assayed by Transwell assays. (D, F) MDA-MB-231 cells were treated with PTX (5 nM), RSL3 (0.5 μM) or their combination for 24 h. Scale bar: 100 μm. (E, G) MDA-MB-468 cells were treated with PTX (5 nM), RSL3 (0.1 μM), or their combination for 24 h. Scale bar: 200 μm. The numbers of migrated and invaded cells were plotted in histograms. * $P < 0.05$, ** $p < 0.01$, *** $p < 0.001$.

DEVD-CHO, necrosis inhibitor necrostatin-1, autophagy inhibitor 3-methyladenine (3-MA), ferroptosis-specific inhibitors ferrostatin-1 (Fer-1) and liproxstatin-1 (LIP), and the iron chelator deferoxamine (DFO). The results demonstrated that Fer-1, DFO and LIP can partially reverse PTX- and RSL3-induced death in TNBC cells (Fig. 2A and B). Therefore, we infer that the type of cell death induced by PTX and RSL3 might be ferroptosis. The essential characteristics of ferroptosis are iron accumulation and lipid peroxidation⁷. Therefore, the intracellular Fe²⁺ levels in MDA-MB-231 and MDA-MB-468 cells were determined with the Fe²⁺ probe FerroOrange. Compared with cells treated with PTX or RSL3 alone, cells treated with the combination of PTX and RSL3 presented stronger orange fluorescence (Fig. 2C). Two indicators of ferroptotic lipid peroxidation in MDA-MB-231 and MDA-MB-468 cells were subsequently examined, namely, lipid ROS accumulation and malondialdehyde (MDA) levels. The intracellular lipid ROS levels were detected with the C11-BODIPY 581/591 lipid peroxidation probe²². Consistent with our anticipated results, a significant increase in lipid ROS accumulation was observed following the combination of PTX and RSL3 (Fig. 2D). Furthermore, MDA levels also increased significantly after the combination of PTX and RSL3 in MDA-MB-231 and MDA-MB-468 cells (Fig. 2E). In summary, our results suggest that ferroptosis may be induced in the TNBC cell lines MDA-MB-231 and MDA-MB-468 upon combination treatment with PTX and RSL3.

Transcriptomics reveals the molecular mechanism by which RSL3 enhances the chemosensitivity of TNBC cells to PTX

To further explore the molecular mechanism by which RSL3 enhances the chemosensitivity of TNBC to PTX, we performed quantitative transcriptomic sequencing (RNA-seq) on MDA-MB-231 cells treated with PTX (5 nM), RSL3 (0.5 µM), or their combination for 24 h. With a series of differentially expressed genes identified, we found that the expression of ERG1, the chemokines CXCL2 and CXCL8, and the inflammatory factors IL-6 and IL-1β in the medication group was significantly increased (Fig. 3A and B). Based on KEGG enrichment analysis of the differential genes among the PTX and RSL3 alone groups and the combination treatment group, we found that the combination treatment group induced gene expression, which was highly related to ferroptosis (Fig. 3C and D). Gene set enrichment analysis (GSEA) revealed that the therapeutic effect of PTX and/or RSL3 on TNBC was mainly enriched in the NF-κB signalling pathway (Fig. 3F). Immune score analysis revealed that M1-type macrophages were significantly increased in the combination treatment group (Fig. 3E). In summary, the transcriptomics results indicated that RSL3 increased the chemosensitivity of TNBC cells to PTX by activating the NF-κB signalling pathway, leading to an increase in the levels of related cytokines.

Combination treatment with PTX and RSL3 activates the NF-κB signalling pathway and promotes TNBC cells death

The NF-κB signalling pathway is a classical inflammatory signalling pathway, and BAY11-7082 is an inhibitor of this pathway²³. NF-κB can be activated by cytokines such as EGR1, CXCL8, and IL-6²⁴. To validate the RNA-seq results, we treated MDA-MB-231 and MDA-MB-468 cells with the NF-κB pathway inhibitor BAY11-7082 combined with PTX and RSL3 to examine cell viability. The results suggested that the addition of the NF-κB signalling pathway inhibitor BAY11-7082 partially reversed the cell death induced by the combination of PTX and RSL3 in both MDA-MB-231 and MDA-MB-468 cells (Fig. 4A). Moreover, after the combination treatment, the expression of EGR1 and cytokines such as CXCL2, CXCL8, IL-6, and IL-1β increased, and this trend could be partially reversed by the NF-κB signalling pathway inhibitor BAY11-7082. The results were verified at the mRNA and protein levels (Fig. 4B and C). The p65 Ser536 site is a key effector site in the NF-κB signalling pathway and plays an important role in tumorigenesis^{25–28}. The effects of PTX combined with RSL3 on changes in NF-κB expression were validated at the protein level. As shown in Fig. 4D, the combination treatment group presented an increased level of protein phosphorylation at the p65 Ser536 site. Additionally, the expression of the ferroptosis suppressor protein GPX4 decreased in the combination treatment group, further confirming the induction of ferroptosis. The effects on both the p65 Ser536 site and GPX4 could be reversed by the NF-κB inhibitor. These results indicated that the combination of PTX and RSL3 activated the NF-κB signalling pathway to induce ferroptosis in TNBC cells, which was consistent with our transcriptome sequencing results.

RSL3 enhances the chemosensitivity of TNBC to PTX in vivo

To further evaluate whether RSL3 enhances the chemosensitivity of TNBC to PTX in vivo, an MDA-MB-231 xenograft model in severely immunocompromised mice was established. Tumours were implanted in the right mammary fat pads of the mice, and 10 days after implantation, the mice were randomly divided into five groups and administered the drugs intraperitoneally. The experimental scheme is depicted in Fig. 5A. All mice survived well after cell implantation and treatment. After 18 days of treatment, the tumour sizes in the RSL3, PTX, and combination treatment groups gradually decreased compared with those in the control group. Notably, the combination of the two drugs resulted in the greatest reduction in tumour size (Fig. 5B–D), without toxicity and side effects on the organs (Fig. 5F). There were no significant changes in body weight or daily food intake between the control and treatment groups (Fig. 5E). The immunohistochemical results revealed that the expression levels of Ki67 and GPX4 in the combination group were significantly reduced (Fig. 5G). The expression of p65 and p-p65 was increased in the combination group, but the increase in p-p65 expression was more significant (Supplementary Fig. S5). These results confirmed that RSL3 could serve as a chemotherapy sensitizer for TNBC to PTX in vivo and that its combination with PTX produced synergistic antiproliferative effects without toxicity or side effects.

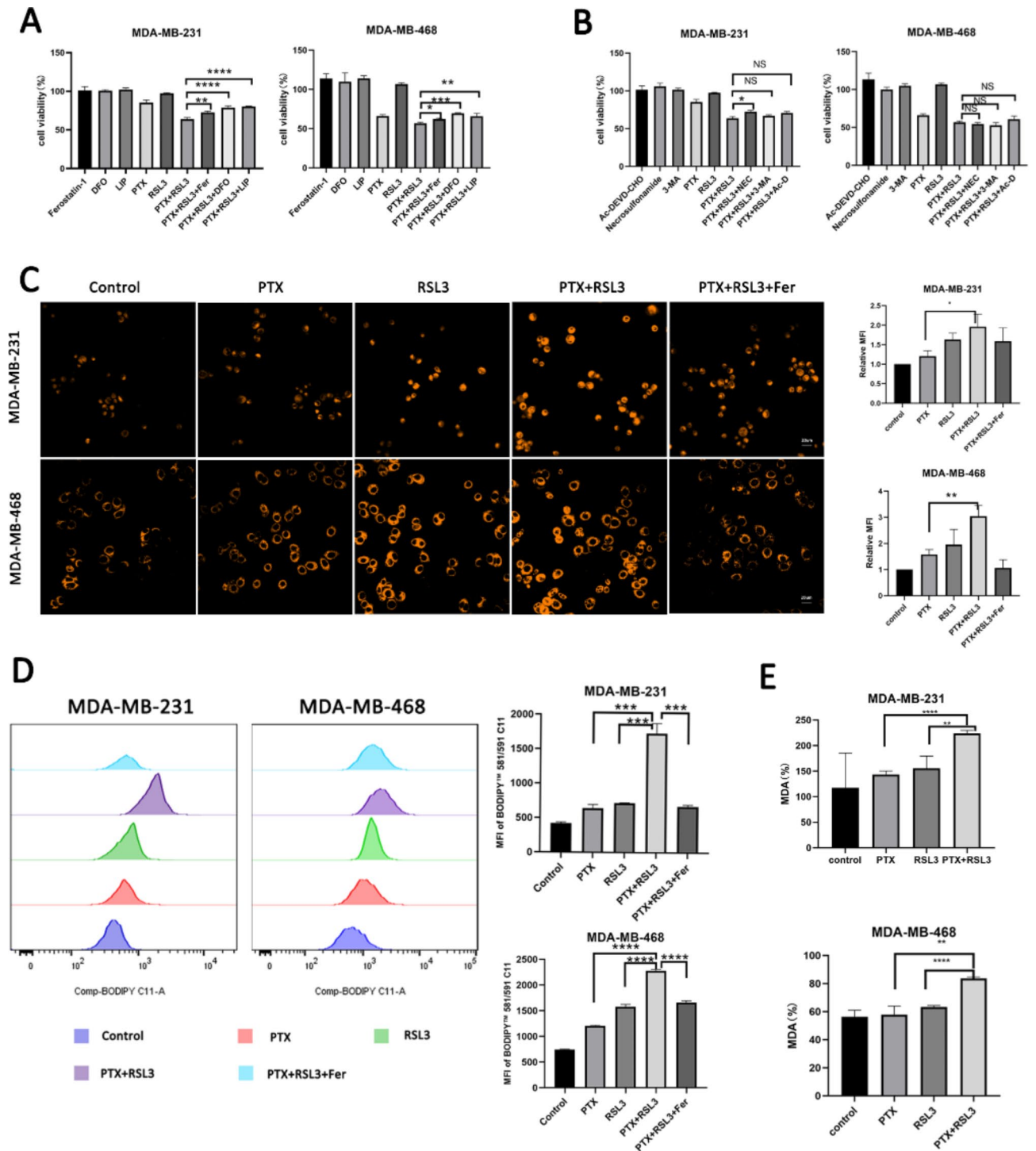


Fig. 2. RSL3 enhances the chemosensitivity of TNBC cells to PTX by inducing ferroptosis. (A, B) MDA-MB-231 cells were treated with PTX (5 nM) and RSL3 (0.5 μ M) combined with Ac-DEVD-CHO (20 μ M), necrostatin-1 (10 μ M), 3-MA (10 μ M), ferrostatin-1 (Fer-1) (10 μ M), liproxstatin-1 (LIP) (200 nM), or deferoxamine (DFO) (5 μ M) for 24 h, and cell viability was assayed using the CCK-8 assay. MDA-MB-468 cells were treated with PTX (5 nM) and RSL3 (0.1 μ M) combined with the same inhibitors for 24 h, and cell viability was also assayed using the CCK-8 assay. (C) The level of Fe²⁺ was measured by FerroOrange. Scale bar: 50 μ m. (D) Cellular lipid ROS levels were analysed by flow cytometry. (e) Intracellular MDA levels were measured using the MDA detection kit. ** $P < 0.01$; * $P < 0.05$; **** $p < 0.0001$; *** $p < 0.001$. NS: Not significant.

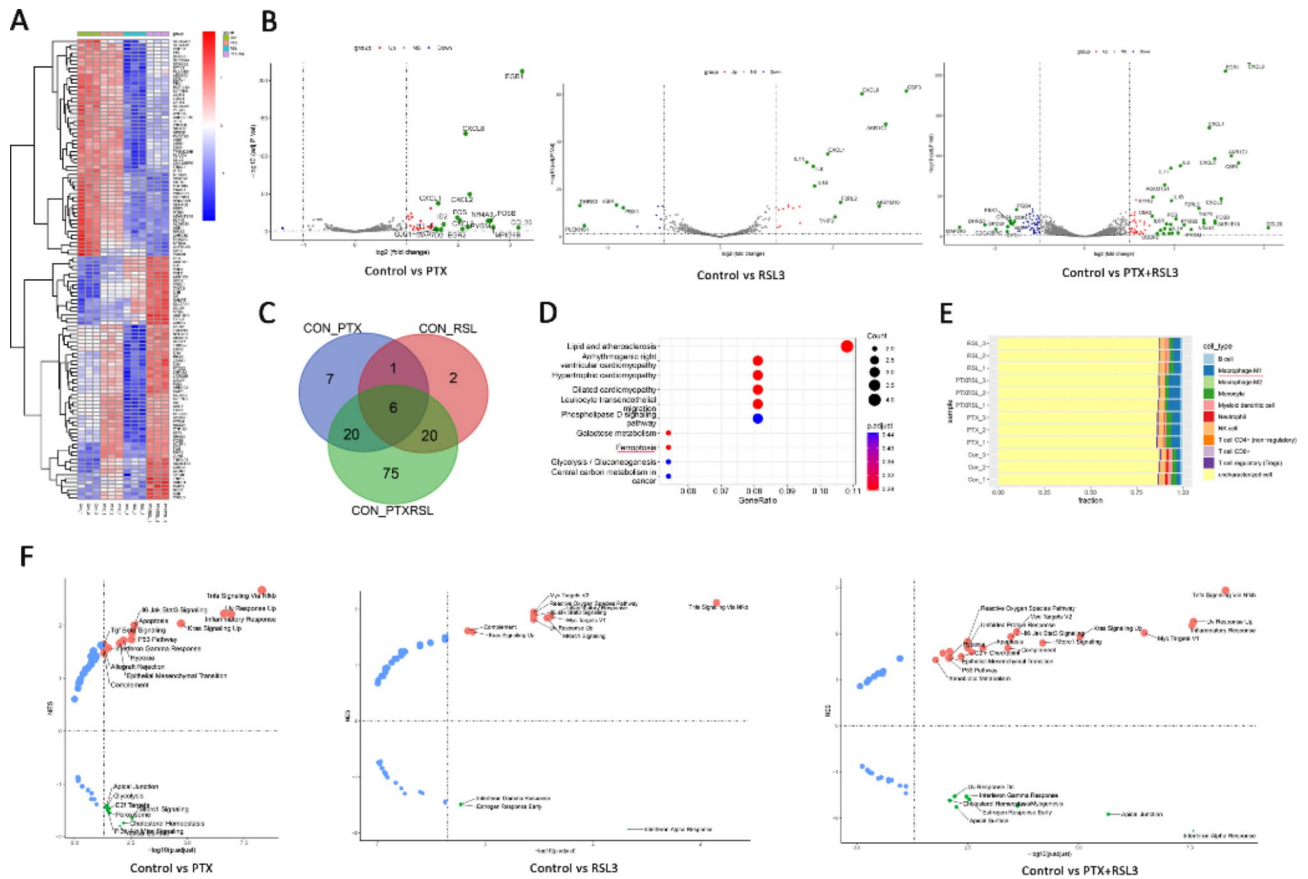


Fig. 3. Transcriptomics reveals the molecular mechanism by which RSL3 enhances the chemosensitivity of TNBC cells to PTX. (A, B) Heatmaps and volcano plots depict the expression of differentially expressed genes among the different treatment groups, with red representing highly expressed genes and blue representing genes with low expression. (C) A Venn diagram shows overlapping and unique genes among the different treatment groups. (D) A bubble chart presents the results of the KEGG enrichment analysis of 75 differentially expressed genes in the Venn diagram, with the size of the circle indicating the number of enriched genes in each project and each colour representing a different p value (www.kegg.jp/kegg/kegg1.html). (E) The infiltration of immune cells in different groups. (F) GSEA pathway enrichment analysis of cancer-related genes, with red circles representing significantly upregulated pathways (www.kegg.jp/kegg/kegg1.html).

Discussion

Our experiments demonstrated that combination treatment with PTX and RSL3 significantly inhibited TNBC cell viability, as well as its clonogenic ability, migration, and invasiveness, with the inhibitory effect proven to be synergistic.

TNBC, a refractory type of breast cancer, has unsatisfactory treatment effects and a poor prognosis. Despite the limited therapeutic efficacy of PTX treatment for TNBC owing to chemotherapy resistance and associated side effects, PTX-based chemotherapy continues to serve as the primary treatment for this subtype of breast cancer²⁹. Therefore, much research has been conducted on PTX sensitization in TNBC chemotherapy. Xu et al.³⁰ reported that TRAF6 can increase the chemosensitivity of TNBC to PTX by regulating glycolysis mediated by PKM2. Zhang et al.³¹ reported that GBP2 enhances the sensitivity of TNBC to PTX by promoting autophagy, inhibiting the PI3K/AKT/mTOR signalling pathway, and binding to ATG2.

Recent studies have shown that activating ferroptosis can effectively prevent tumour progression and can be combined with chemotherapy drugs to increase the sensitivity of tumours to traditional chemotherapy drugs. Compared with single drugs, the combination of PTX and the xCT inhibitor sulfasalazine (SAS) significantly enhances cytotoxicity in ovarian clear cell carcinoma cells, along with a decrease in GPX4 expression, elevated intracellular iron levels, and significant accumulation of lipid ROS, thus resulting in ferroptosis³². In addition, the combination of propofol and PTX at certain concentrations can significantly inhibit the viability of cervical cancer cells, and this inhibitory effect has a synergistic effect³³. Moreover, the ROS levels and Fe²⁺ concentrations also increase accordingly, indicating that propofol enhances the chemosensitivity of cervical cancer cells by inducing ferroptosis³³. Other studies reported that the combination of low-concentration PTX and RSL3 can induce ferroptosis in mutant p53 hypopharyngeal squamous cell carcinoma, synergistically inhibiting tumour growth³⁴.

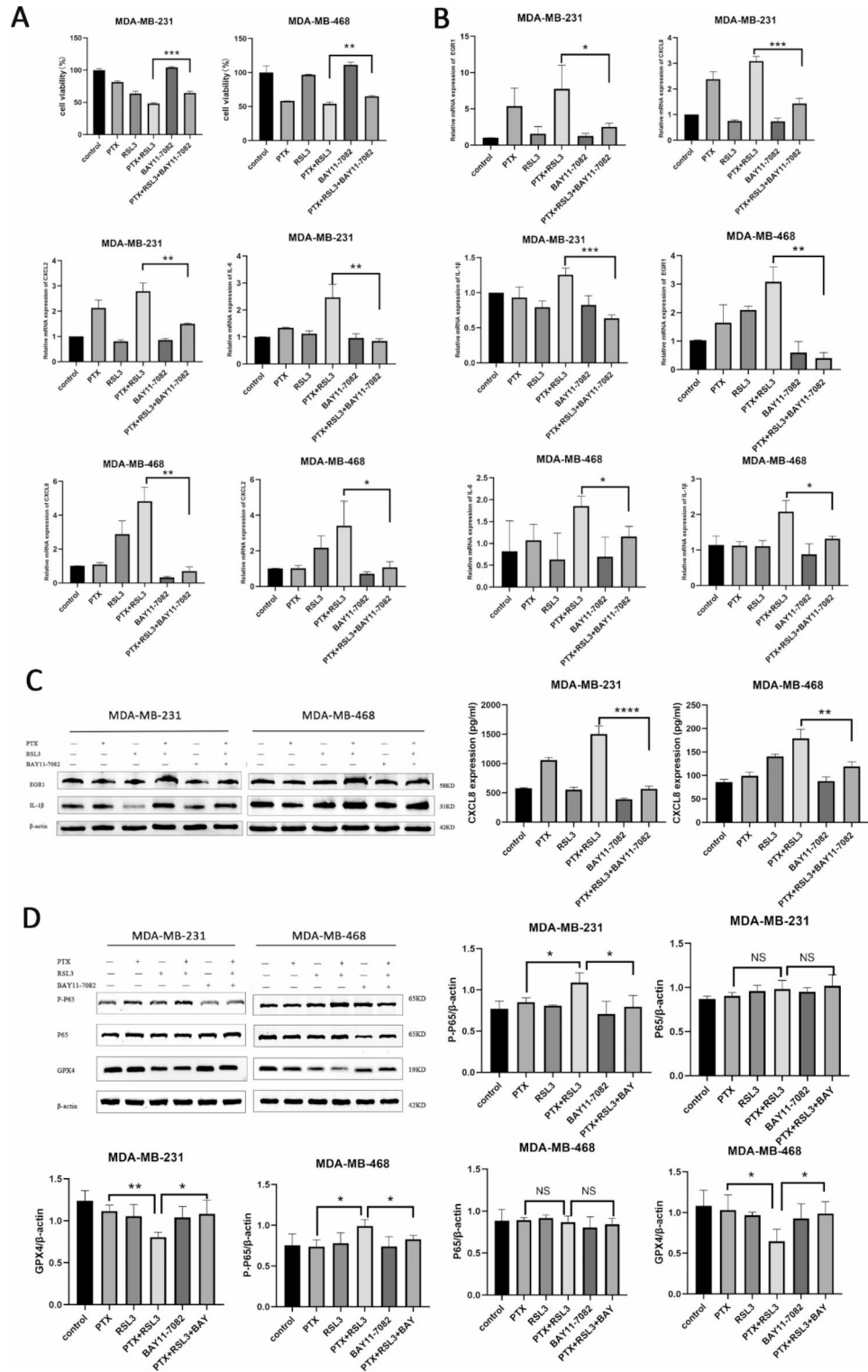


Fig. 4. Combination treatment with PTX and RSL3 activates NF-κB and promotes TNBC cell death. **(A)** The viability of MDA-MB-231 and MDA-MB-468 cells was assayed using the CCK-8 assay after combination treatment with PTX or RSL3 and an NF-κB inhibitor for 24 h. **(B)** After the treatments, the expression levels of cytokines were detected by RT-qPCR. **(C)** After the treatments, the expression levels of cytokines were detected by Western blotting and ELISA. **(D)** The protein expression levels of P65, P-P65 and GPX4 were measured by Western blotting, and a grayscale map of protein expression is displayed. ** $P < 0.01$; * $P < 0.05$; **** $p < 0.0001$; *** $p < 0.001$. NS: Not significant.

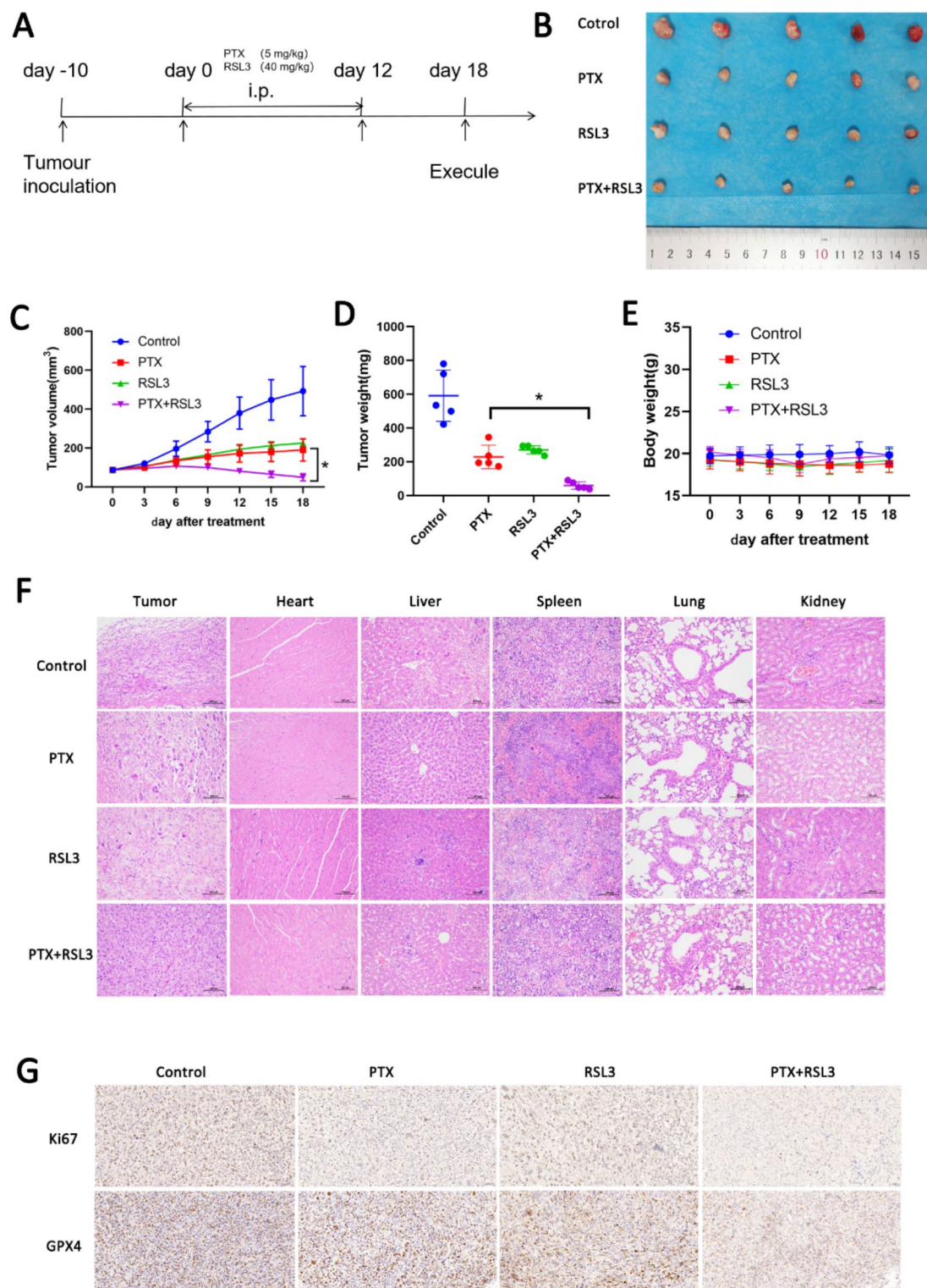


Fig. 5. RSL3 enhanced the chemosensitivity of TNBC to PTX in vivo. **(A)** Experimental design. Day -10: MDA-MB-231 cells (6×10^6 cells/100 μ l) were inoculated subcutaneously into the right mammary fat pads of severely immunocompromised mice. Day 0: paclitaxel (5 mg/kg) and RSL3 (40 mg/kg) were administered via intraperitoneal injection at a volume of 100 μ l, with administration every 3 days. **(B)** Anatomical images of excised tumours on Day 18. **(C)** Volumes of excised tumours on Day 18. **(D)** The tumour weights of the mice in each group were calculated every 3 days. **(E)** The body weights of the mice in each group were calculated every 3 days. **(F)** Haematoxylin and eosin staining of mouse organs and tumours; scale bar: 100 μ m. **(G)** Ki67 and GPX4 expression was detected by immunohistochemical staining; scale bar: 50 μ m. * $P < 0.05$.

To clarify whether the combination of drugs can induce ferroptosis in tumour cells, we detected ferroptosis-related markers, and the results revealed significant changes in the levels of markers such as Fe^{2+} , lipid ROS, MDA and GPX4 in the drug combination group. Subsequently, apoptosis inhibitors, necrosis inhibitors, autophagy inhibitors, ferroptosis-specific inhibitors, and iron chelators were added to the combination treatment group to test cell viability. In addition to ferroptosis inhibitors, other types of cell death inhibitors could not reverse the inhibitory effect of combination treatment on cell viability, indicating that combination treatment can reduce the viability of TNBC cells by inducing ferroptosis.

Mechanistically, through transcriptome sequencing, we identified a series of differentially expressed genes, discovering that EGR1 and some cytokines, such as CXCLs, were significantly upregulated in the drug-treated group. Upon enrichment analysis of these differentially expressed genes, we found a strong correlation with ferroptosis and further revealed that the combination therapy effect on TNBC was primarily enriched in the NF- κ B signalling pathway. Validation via RT-qPCR confirmed our RNA-seq results, and Western blot experiments revealed that the combination treatment significantly increased the phosphorylation level of the p65 protein at the Ser536 site and decreased the expression of the ferroptosis-inhibiting protein GPX4. Both protein expression changes could be reversed by NF- κ B inhibitors, which also reversed the inhibitory effect of the drugs on TNBC cell viability. Thus, the crucial role of the NF- κ B signalling pathway in enhancing the chemosensitivity of TNBC cells to PTX through RSL3-induced ferroptosis has been proven by these results.

P65, an effector molecule of the canonical NF- κ B signalling pathway, is vital for tumour survival²⁷. To date, a total of 12 phosphorylation sites have been identified in p65, including 9 serine sites and 3 threonine sites²⁷. Among them, phosphorylated p65 (Ser536) is a recognized indicator of NF- κ B signal transduction activity^{25,26}. The phosphorylation and activation of the p65 protein at the Ser536 site exerts a tumour-suppressive effect in malignancies, such as those associated with colon, breast and cervical cancers^{27,28}. Moreover, RSL3 has been shown to activate the NF- κ B signalling pathway, further reducing GPX4 transcription and inducing ferroptosis in glioblastoma³⁵, which is consistent with our findings. As a cancer suppressor gene, EGR1 functions as a nuclear protein with transcriptional regulatory roles, where its activated target gene products are essential for both differentiation and mitosis³⁶. PTX can promote an increase in EGR1 expression, which participates in paclitaxel-induced breast cancer cell death³⁶. In addition, granulosa cell apoptosis can be promoted by increased EGR1 expression via the NF- κ B signalling pathway²⁴. EGR1 can also interact with NF- κ B by forming an NF- κ B/EGR1 complex, which plays an important role in the treatment of prostate cancer³⁷. Research has indicated that NF- κ B signalling pathway activation leads to the upregulation of inflammation-related factors (e.g., IL-1 β , IL-6, and TNF α), which in turn can further activate the NF- κ B signalling pathway^{38,39}. Similarly, increased lipid peroxidation after ferroptosis in tumour cells can activate various inflammatory cells and pathways, resulting in an increase in inflammatory factors, which in turn exacerbates intracellular oxidative stress and lipid peroxidation⁴⁰. Therefore, we conclude that the combination of PTX and RSL3 can induce ferroptosis in TNBC cells by activating the NF- κ B signalling pathway, thereby increasing the chemosensitivity of TNBC to PTX.

Ferroptosis is widely recognized as a type of immunogenic cell death (ICD)⁴¹ and is capable of activating the immune system and synergizing with immune checkpoint inhibitors (ICI)^{42–44}. In tumour therapy, it can recruit antigen-presenting cells (APCs) and effector CD4+ and CD8+ T cells to further kill tumour cells by releasing various damage-associated molecular patterns (DAMPs)^{45–47}. TNBC, which is considered an immunologically “cold” tumour, has a poor immunotherapy response due to the lack of immune cell infiltration in its immune microenvironment⁴⁷. However, the antigens and adjuvant molecules with immune-activating capabilities generated after ICD can transform the tumour microenvironment from a non-inflammatory “cold” to an inflammatory “hot” immune state, enhancing immune cell activation and ultimately producing more effective tumour cell killing⁴⁷. In our study, the immune infiltration scores of the RNA-seq data revealed a significant increase in M1 macrophages in the combination treatment group. Macrophages consist of M1 and M2 types, of which M1 macrophages distinguish between tumour cells and normal cells and ultimately kill tumour cells, and M2 macrophages promote tumour development^{48,49}. Ferroptosis in tumour cells has been reported to induce macrophage polarization towards the M1 phenotype, enhancing antitumour capabilities^{50,51}. In breast cancer, the induction of ferroptosis can promote the polarization of tumour-associated macrophages towards the antitumour M1 phenotype^{52,53}. It has also been reported that macrophages can phagocytose dead tumour cells and enhance the effects of chemotherapy and radiotherapy^{42–44}. However, further studies should be conducted to validate and explore the role and mechanism of ferroptosis in immunotherapy for TNBC as well as the impact and regulatory mechanisms of increased M1 macrophages on the tumour microenvironment and traditional treatment response. This study provides theoretical and experimental insights for further optimizing treatment strategies and improving treatment outcomes.

In conclusion, our study revealed that the combination of PTX and RSL3 can significantly inhibit the activity of TNBC cells and, for the first time, that their combination activates NF- κ B to induce ferroptosis, thus increasing the chemosensitivity of TNBC to PTX. This discovery reveals a new anticancer mechanism that combines traditional chemotherapy drugs with ferroptosis inducers and is expected to contribute to the development of more effective treatment strategies for TNBC patients.

Methods

Cell lines

The TNBC cell lines MDA-MB-231 and MDA-MB-468 were purchased from the Chinese Academy of Sciences. MDA-MB-231 cells were cultured in RPMI 1640 (Gibco) containing 10% foetal bovine serum (Biological Industries) and 1% penicillin-streptomycin (Cytiva) and incubated in a humidified incubator at 37 °C with 5% CO_2 . MDA-MB-468 cells were cultured in L15 medium (iCell) supplemented with 10% foetal bovine serum and 1% penicillin-streptomycin (Cytiva) and incubated in a humidified incubator at 37 °C without CO_2 .

Reagents and antibodies

PTX (S1150) was purchased from Selleck Chemicals (Houston, TX, USA), while RSL3 (HY-100218A) and the NF- κ B inhibitor BAY 11-7082 (HY-13453) were obtained from MedChemExpress (Monmouth Junction, NJ, USA), as were necrostatin-1 (HY-15760), Ac-DEVD-CHO (HY-P1001), ferrostatin-1 (Fer-1) (HY-100579), and 3-methyladenine (3-MA) (HY-19312). NF- κ B p65 (D14E12) rabbit monoclonal antibody (8242), phospho-NF- κ B p65 (Ser536) rabbit monoclonal antibody (3033), and anti-rabbit IgG (H + L) (DyLight™ 800 4X PEG Conjugate) rabbit secondary antibody (5151) were purchased from Cell Signaling Technology (CST). The GPX4 rabbit monoclonal antibody (T56959) was obtained from Abmat. An EGR1 rabbit monoclonal antibody (JE57-62) and an IL-1 β rabbit monoclonal antibody (JJ087-3) were obtained from HUABIO. β -actin was purchased from Servicebio (GB15003-100).

Cell viability assay

Cell viability was determined via the Cell Counting Kit-8 (CCK-8; Bimake, Houston, TX, USA). The cells were seeded in 96-well plates at a density of 6000–8000 cells per well and treated as indicated for 24, 48, or 72 h. Then, 10 μ L of CCK-8 solution was added to each well, and the cells were incubated for another 2–4 h at 37 °C. The absorbance of the mixture was measured at 450 nm using a BioTak Elx808.

Colony formation assay

Cells (1000 per well) were seeded into 6-well plates. After two weeks, the colonies were fixed in methanol and stained with 0.5% crystal violet for 30 min, and individual colonies containing more than 50 cells were counted.

Transwell migration and invasion assays

Cell migration and invasion were evaluated using tissue culture plate inserts (LABSELECT, China). For the cell migration assay, a cell suspension of 8×10^4 cells in 200 μ L of 2% FBS was added to the upper chamber of the insert, and media containing 20% FBS (500 μ L) was added to the lower chamber. After 24 h of incubation, the membrane of the insert was fixed in methanol for 30 min and stained with crystal violet solution for 30 min. Then, the cells on the upper filter surface were wiped away with a cotton swab, and the remaining cells on the opposite side of the filter were counted at 10 \times magnification. For the invasion assay, 50 μ L of Matrigel (diluted 1:10) was precoated in the upper chamber and incubated at 37 °C for 4 h.

Lipid reactive oxygen species (ROS) level assay

C11-BODIPY 581/591 (D3861, Thermo Fisher Scientific) was utilized to detect lipid ROS²². C11-BODIPY (1 μ M) was incubated with the cells in media at 37 °C for 30 min. After incubation, the cells were washed twice with PBS, resuspended in PBS, and then analysed via flow cytometry (Becton CYTOMINCS FC500, USA). The results were analysed using FlowJo-V10.8.1 software.

Malondialdehyde (MDA) assay

MDA levels in TNBC cells were measured using a Lipid Peroxidation MDA Assay Kit (BC0025, Solarbio, China). The absorbance was measured at 532 nm and 600 nm using a microplate reader. The protein concentration of the samples was determined via a BCA assay kit (P0010, Beyotime, China). The data of each sample were normalized, and the MDA content was calculated according to the manufacturer's instructions for the MDA Assay Kit: MDA (nmol/mg prot) = $53.763 \times \Delta A / \text{Cpr}$.

Intracellular iron assay

The intracellular level of iron was detected via FerroOrange (F374, Dojindo, Japan)⁵⁴. The cells were seeded in confocal dishes and incubated for 24 h. The cells were subsequently treated with FerroOrange (1 mM) in PBS and incubated at 37 °C for 30 min. Fluorescence detection was then performed using a confocal microscope (Olympus FV1000, Japan).

RNA-seq and bioinformatic analysis

The Illumina sequencing platform (Personal Biotechnology Cp.) was used to perform high-throughput RNA-seq on MDA-MB-231 cell samples with and without PTX or/and RSL3. The bioinformatic analysis was performed using R program (version R 4.3.2). The sequence alignment results were screened to identify differentially expressed genes using the DESeq package, and the screening criteria were $|\log_2\text{FC}| \geq 1$ and adjusted P value < 0.05. We mapped all the genes to terms in the Gene Ontology database and calculated the number of differentially enriched genes associated with each term. Differential expression analysis was performed using DESeq2 (<http://bioconductor.org/packages/DESeq2/>). A heatmap was visualized using the heatmap.2 package. Volcano plots were generated using the R package Enhanced volcano. Venn diagrams were generated using the Venn diagram tool (<http://bioinformatics.psb.ugent.be/webtools/Venn/>). The clusterProfiler (v4.6.0) package (<https://guangchuangyu.github.io/software/clusterProfiler>) was used to conduct KEGG enrichment analysis of differential gene pathways (<https://www.kegg.jp/kegg/kegg1.html>), with a focus on significantly enriched pathways with P values < 0.05. The Gene Set Enrichment Analysis (GSEA) (v4.1.0) tool was used for enrichment analysis of all genes, and a GSEA enrichment analysis pathway map was drawn using the R program.

Real-time quantitative reverse transcription PCR (qRT-PCR) analysis

Total RNA was extracted from cultured cells via an EZ-press RNA Purification Kit (EZBioscience) and then reverse transcribed into cDNA using Colour Reverse Transcription Kit with gDNA Remover (EZBioscience). The qRT-PCR analysis was performed using 2 \times Colour SYBR Green qPCR Master Mix (EZBioscience) on a real-time quantitative PCR instrument (C1000 Thermal Cycle, Bio-Rad, USA). With GAPDH as an internal

reference, the sequences of primers used for the qRT-PCR of the genes examined are listed in Supplementary Table S1.

Western blotting

Proteins were lysed using RIPA buffer (Beyotime, China) containing a protease/phosphatase inhibitor mixture and quantified using a BCA protein assay kit (Beyotime, China). The proteins were separated by SDS-PAGE and transferred onto PVDF membranes. The membranes were blocked with 5% skim milk for 1 h at room temperature and incubated with primary antibodies (1:1000) overnight at 4 °C. The target proteins were incubated with secondary antibodies (1:10,000) for 1 h. The membranes were subsequently washed three times with TBST solution and finally imaged using the Odyssey system (LI-COR Odyssey, United States).

Enzyme-linked immunosorbent assay (ELISA)

After drug treatment, the intracellular CXCL8 levels were measured using the appropriate ELISA kit (ABclonal, China) according to the manufacturer's protocol. The absorbance of the mixture was measured at 450 nm and 570 nm with a BioTak Elx808.

Xenograft tumour model

Female NOD-SCID mice (4–5 weeks old, 18–22 g) were purchased from Beijing Wei Tong Li Hua Laboratory Animal Technology (Licence number: SCXK [Beijing] 2021-0006). The mice were housed in the Experimental Animal Centre of the Basic Medical School of Jilin University (SPF level) following national and international guidelines. This experiment was approved by the Experimental Animal Ethics Committee of the Basic Medical School of Jilin University (ethical number: NO.2014311), and the study was performed in accordance with relevant guidelines and regulations. The study is reported in accordance with the Animal Research: Reporting of In Vivo Experiments guidelines. All animals were maintained at a constant temperature, 40–70% humidity, and a 12:12 light–dark cycle with air exchange. The mice had ad libitum access to food and water. All mice were deeply anaesthetized by sodium pentobarbital injection and euthanized by cervical dislocation. All aspects of animal welfare, including minimizing pain and suffering and the use of painkillers or anaesthetics, were considered. After the experimental objectives were met, the animals were treated in a scientific and humane manner to minimize their panic and suffering, and euthanasia was performed gently and quickly.

A suspension of MDA-MB-231 cells (6×10^6 cells/100 μ l) was injected subcutaneously into the right mammary fat pads of 5-week-old female NOD-SCID mice with severe immune deficiency. The mice were randomly divided into four groups (5 mice/group): (1) the control group, (2) the PTX group, (3) the RSL3 group, and (4) the PTX + RSL3 group. Both PTX (5 mg/kg) and RSL3 (40 mg/kg) were administered via intraperitoneal injection in a volume of 100 μ l every 3 days for a total of 5 administrations. The control group was treated with an equal volume (100 μ l) of saline. The tumour volume was calculated as $0.5 \times \text{length} \times \text{width}^2$. After 18 days of treatment, the mice were sacrificed (the mice were deeply anaesthetized by sodium pentobarbital injection and euthanized by cervical dislocation), and the tumours were excised and weighed. Haematoxylin and eosin and immunohistochemical staining were subsequently conducted on tumour tissues obtained from different treatment groups.

Immunohistochemistry (IHC)

Xenograft tumour tissues were fixed, dehydrated, embedded in paraffin, and sectioned (4 μ m). The slides were incubated with the following primary antibodies: Ki67 (1:1000), GPX4 (1:1000), p65 (1:400) and p-p65 (1:100).

Statistical analysis

Statistical analysis was performed using GraphPad Prism 8.0 software (San Diego, CA, USA). Differences between the control and experimental groups were considered statistically significant and highly significant at $P < 0.05$ and $P < 0.01$ respectively. P values were analysed using the Student's t test or one-way ANOVA. All data were derived from at least three independent experiments.

Data availability

The original contributions presented in the study are included in the article/supplementary material, further inquiries can be directed to the corresponding authors. Sequence data that support the findings of this study have been deposited in the Database. (<https://www.jianguoyun.com/p/DREjf8YQyvXtDBiyruAFIAA>).

Received: 3 June 2024; Accepted: 6 January 2025

Published online: 11 January 2025

References

- Dietze, E. C., Sistrunk, C., Miranda-Carboni, G., O'Regan, R. & Seewaldt, V. L. Triple-negative breast cancer in African-American women: Disparities versus biology. *Nat. Rev. Cancer* **15**, 248–254 (2015).
- Harbeck, N. et al. Breast cancer. *Nat. Rev. Dis. Primers* **5**, 66 (2019).
- Garrido-Castro, A. C., Lin, N. U. & Polyak, K. Insights into molecular classifications of triple-negative breast cancer: Improving patient selection for treatment. *Cancer Discov.* **9**, 176–198 (2019).
- Groheux, D. et al. Prognostic impact of 18F-FDG PET/CT staging and of pathological response to neoadjuvant chemotherapy in triple-negative breast cancer. *Eur. J. Nucl. Med. Mol. Imaging* **42**, 377–385 (2015).
- Li, Y. et al. Recent advances in therapeutic strategies for triple-negative breast cancer. *J. Hematol. Oncol.* **15**, 121 (2022).
- Schettini, F., Giuliano, M., De Placido, S. & Arpino, G. Nab-paclitaxel for the treatment of triple-negative breast cancer: Rationale, clinical data and future perspectives. *Cancer Treat. Rev.* **50**, 129–141 (2016).

7. Stockwell, B. R. Ferroptosis turns 10: Emerging mechanisms, physiological functions, and therapeutic applications. *Cell* **185**, 2401–2421 (2022).
8. Yang, W. S. & Stockwell, B. R. Synthetic lethal screening identifies compounds activating iron-dependent, nonapoptotic cell death in oncogenic-RAS-harboring cancer cells. *Chem. Biol.* **15**, 234–245 (2008).
9. Zheng, J. & Conrad, M. The metabolic underpinnings of ferroptosis. *Cell Metab.* **32**, 920–937 (2020).
10. Lei, G. et al. The role of ferroptosis in ionizing radiation-induced cell death and tumor suppression. *Cell Res.* **30**, 146–162 (2020).
11. Guo, J. et al. Ferroptosis: A novel anti-tumor action for cisplatin. *Cancer Res. Treat.* **50**, 445–460 (2018).
12. Sun, X. et al. Activation of the p62-Keap1-NRF2 pathway protects against ferroptosis in hepatocellular carcinoma cells. *Hepatology* **63**, 173–184 (2016).
13. Wang, W. et al. CD8(+) T cells regulate tumour ferroptosis during cancer immunotherapy. *Nature* **569**, 270–274 (2019).
14. Lv, C. et al. Low-dose paclitaxel inhibits tumor cell growth by regulating glutaminolysis in colorectal carcinoma cells. *Front. Pharmacol.* **8**, 244 (2017).
15. Lorito, N. et al. FADS1/2 control lipid metabolism and ferroptosis susceptibility in triple-negative breast cancer. *EMBO Mol. Med.* **16**, 1533–1559 (2024).
16. Zhang, Y. et al. Imidazole ketone erastin induces ferroptosis and slows tumor growth in a mouse lymphoma model. *Cell Chem. Biol.* **26**, 623–633.e9 (2019).
17. Liang, C., Zhang, X., Yang, M. & Dong, X. Recent progress in ferroptosis inducers for cancer therapy. *Adv. Mater.* **31**, e1904197 (2019).
18. Ueda, N. & Takasawa, K. Impact of inflammation on ferritin, hepcidin and the management of iron deficiency anemia in chronic kidney disease. *Nutrients* **10**, 1173 (2018).
19. Yu, H., Lin, L., Zhang, Z., Zhang, H. & Hu, H. Targeting NF- κ B pathway for the therapy of diseases: Mechanism and clinical study. *Signal Transduct. Target. Ther.* **5**, 209 (2020).
20. Yan, N., Xu, Z., Qu, C. & Zhang, J. Dimethyl fumarate improves cognitive deficits in chronic cerebral hypoperfusion rats by alleviating inflammation, oxidative stress, and ferroptosis via NRF2/ARE/NF- κ B signal pathway. *Int. Immunopharmacol.* **98**, 107844 (2021).
21. Ianevski, A., Giri, A. K. & Aittokallio, T. SynergyFinder 3.0: An interactive analysis and consensus interpretation of multi-drug synergies across multiple samples. *Nucleic Acids Res.* **50**, W739–W743 (2022).
22. Cheloni, G. & Slaveykova, V. I. Optimization of the C11-BODIPY(581/591) dye for the determination of lipid oxidation in *Chlamydomonas reinhardtii* by flow cytometry. *Cytometry A* **83**, 952–961 (2013).
23. Chen, Y., Fang, Z. M., Yi, X., Wei, X. & Jiang, D. S. The interaction between ferroptosis and inflammatory signaling pathways. *Cell Death Dis.* **14**, 205 (2023).
24. Yuan, S. et al. Age-associated up-regulation of EGR1 promotes granulosa cell apoptosis during follicle atresia in mice through the NF- κ B pathway. *Cell Cycle* **15**, 2895–2905 (2016).
25. Sakurai, H., Chiba, H., Miyoshi, H., Sugita, T. & Toriumi, W. I κ B kinases phosphorylate NF- κ B p65 subunit on serine 536 in the transactivation domain. *J. Biol. Chem.* **274**, 30353–30356 (1999).
26. Li, Q. & Verma, I. M. NF- κ B regulation in the immune system. *Nat. Rev. Immunol.* **2**, 725–734 (2002).
27. Bu, Y. et al. A phosphomimetic mutant of RelA/p65 at Ser536 induces apoptosis and senescence: An implication for tumor-suppressive role of Ser536 phosphorylation. *Int. J. Cancer* **138**, 1186–1198 (2016).
28. Pan, X. et al. STC1 promotes cell apoptosis via NF- κ B phospho-P65 Ser536 in cervical cancer cells. *Oncotarget* **8**, 46249–46261 (2017).
29. Mahtani, R. et al. Advances in therapeutic approaches for triple-negative breast cancer. *Clin. Breast Cancer* **21**, 383–390 (2021).
30. Xu, H. et al. TRAF6 promotes chemoresistance to paclitaxel of triple negative breast cancer via regulating PKM2-mediated glycolysis. *Cancer Med.* **12**, 19807–19820 (2023).
31. Zhang, W. et al. GBP2 enhances paclitaxel sensitivity in triple-negative breast cancer by promoting autophagy in combination with ATG2 and inhibiting the PI3K/AKT/mTOR pathway. *Int. J. Oncol.* **64**, 34 (2024).
32. Idei, U., Ohta, T., Yamatani, H., Seino, M. & Nagase, S. Mechanism of cell death by combined treatment with an xCT inhibitor and paclitaxel: An alternative therapeutic strategy for patients with ovarian clear cell carcinoma. *Int. J. Mol. Sci.* **24**, 11781 (2023).
33. Zhao, M. Y., Liu, P., Sun, C., Pei, L. J. & Huang, Y. G. Propofol augments paclitaxel-induced cervical cancer cell ferroptosis in vitro. *Front. Pharmacol.* **13**, 816432 (2022).
34. Ye, J., Jiang, X., Dong, Z., Hu, S. & Xiao, M. Low-concentration PTX And RSL3 inhibits tumor cell growth synergistically by inducing ferroptosis in mutant p53 hypopharyngeal squamous carcinoma. *Cancer Manag. Res.* **11**, 9783–9792 (2019).
35. Li, S. et al. RSL3 drives ferroptosis through NF- κ B pathway activation and GPX4 depletion in glioblastoma. *Oxid. Med. Cell. Longev.* **2021**, 2915019 (2021).
36. Lasham, A. et al. A novel EGR-1 dependent mechanism for YB-1 modulation of paclitaxel response in a triple negative breast cancer cell line. *Int. J. Cancer* **139**, 1157–1170 (2016).
37. Ma, J. et al. Targeted knockdown of EGR-1 inhibits IL-8 production and IL-8-mediated invasion of prostate cancer cells through suppressing EGR-1/NF- κ B synergy. *J. Biol. Chem.* **284**, 34600–34606 (2009).
38. Baeuerle, P. A. & Baltimore, D. NF- κ B: Ten years after. *Cell* **87**, 13–20 (1996).
39. Barnes, P. J. & Karin, M. Nuclear factor- κ B: A pivotal transcription factor in chronic inflammatory diseases. *N. Engl. J. Med.* **336**, 1066–1071 (1997).
40. Chen, X., Kang, R., Kroemer, G. & Tang, D. Ferroptosis in infection, inflammation, and immunity. *J. Exp. Med.* **218**, e20210518 (2021).
41. Wiernicki, B. et al. Cancer cells dying from ferroptosis impede dendritic cell-mediated anti-tumor immunity. *Nat. Commun.* **13**, 3676 (2022).
42. Fucikova, J. et al. Detection of immunogenic cell death and its relevance for cancer therapy. *Cell Death Dis.* **11**, 1013 (2020).
43. Demuynck, R., Efimova, I., Naessens, F. & Krysko, D. V. Immunogenic ferroptosis and where to find it?. *J. Immunother. Cancer* **9**, e003430 (2021).
44. Song, W. et al. Synergistic and low adverse effect cancer immunotherapy by immunogenic chemotherapy and locally expressed PD-L1 trap. *Nat. Commun.* **9**, 2237 (2018).
45. Garg, A. D. & Agostinis, P. Cell death and immunity in cancer: From danger signals to mimicry of pathogen defense responses. *Immunol. Rev.* **280**, 126–148 (2017).
46. Krysko, D. V. et al. Immunogenic cell death and DAMPs in cancer therapy. *Nat. Rev. Cancer* **12**, 860–875 (2012).
47. Gruosso, T. et al. Spatially distinct tumor immune microenvironments stratify triple-negative breast cancers. *J. Clin. Invest.* **129**, 1785–1800 (2019).
48. Pan, Y., Yu, Y., Wang, X. & Zhang, T. Tumor-associated macrophages in tumor immunity. *Front. Immunol.* **11**, 583084 (2020).
49. Mantovani, A., Sozzani, S., Locati, M., Allavena, P. & Sica, A. Macrophage polarization: Tumor-associated macrophages as a paradigm for polarized M2 mononuclear phagocytes. *Trends Immunol.* **23**, 549–555 (2002).
50. Handa, P. et al. Iron alters macrophage polarization status and leads to steatohepatitis and fibrogenesis. *J. Leukoc. Biol.* **105**, 1015–1026 (2019).
51. Zhou, Y. et al. Iron overloaded polarizes macrophage to proinflammation phenotype through ROS/acetyl-p53 pathway. *Cancer Med.* **7**, 4012–4022 (2018).

52. Jiang, Q. et al. Platelet membrane-camouflaged magnetic nanoparticles for ferroptosis-enhanced cancer immunotherapy. *Small* **16**, e2001704 (2020).
53. Wei, Y. et al. Reactive oxygen species / photothermal therapy dual-triggered biomimetic gold nanocages nanoplatform for combination cancer therapy via ferroptosis and tumor-associated macrophage repolarization mechanism. *J. Colloid Interface Sci.* **606**, 1950–1965 (2022).
54. Guo, S. et al. Dihydroartemisinin-loaded magnetic nanoparticles for enhanced chemodynamic therapy. *Front. Pharmacol.* **11**, 226 (2020).

Author contributions

JY, HX and ZY conceived, designed the experiments, and wrote the manuscript. JY, ZY, and CL performed the experiments. JY and CJ analyzed the data. HX and NL contributed to material and analysis tools. All authors read and approved the final manuscript.

Funding

This study was supported by the Department of Science and Technology of Jilin Province (20210203215SF, YDZJ202301ZYTS098, ZYY and Jilin Provincial Research Foundation of China Grants (Nos. 2018SCZ014, 2019SCZ049).

Declarations

Competing interests

The authors declare no competing interests.

Additional information

Supplementary Information The online version contains supplementary material available at <https://doi.org/10.1038/s41598-025-85774-w>.

Correspondence and requests for materials should be addressed to N.L., Z.Y. or H.X.

Reprints and permissions information is available at www.nature.com/reprints.

Publisher's note Springer Nature remains neutral with regard to jurisdictional claims in published maps and institutional affiliations.

Open Access This article is licensed under a Creative Commons Attribution-NonCommercial-NoDerivatives 4.0 International License, which permits any non-commercial use, sharing, distribution and reproduction in any medium or format, as long as you give appropriate credit to the original author(s) and the source, provide a link to the Creative Commons licence, and indicate if you modified the licensed material. You do not have permission under this licence to share adapted material derived from this article or parts of it. The images or other third party material in this article are included in the article's Creative Commons licence, unless indicated otherwise in a credit line to the material. If material is not included in the article's Creative Commons licence and your intended use is not permitted by statutory regulation or exceeds the permitted use, you will need to obtain permission directly from the copyright holder. To view a copy of this licence, visit <http://creativecommons.org/licenses/by-nc-nd/4.0/>.

© The Author(s) 2025